Phase discrimination between δ and η phases in the new nickel-based superalloy VDM Alloy 780 using EBSD

Juhi Sharma, Alexis Nicolaÿ, Marc de Graef, Nathalie Bozzolo

Phase discrimination between δ and η phases in the new nickel-based superalloy VDM Alloy 780 using EBSD

Juhi Sharma[a,*], Alexis Nicolaÿ[a], Marc De Graef[b], Nathalie Bozzolo[a]

[a]*MINES ParisTech, PSL University, Centre de Mise en Forme des Matériaux (CEMEF), CNRS UMR 7635, CS 10207, rue Claude Daunesse, 06904, Sophia Antipolis Cedex, France*
[b]*Department of Materials Science and Engineering, Carnegie Mellon University, 5000 Forbes Avenue, Pittsburgh, PA 15213, USA*

Keywords: EBSD, Phase Discrimination, Dictionary Indexing

Abstract

VDM Alloy 780 is a new nickel-based superalloy developed for higher service temperatures up to 750°C. In addition to fine γ′-Ni_3(Al,Ti) strengthening precipitates, grain boundary precipitates resembling δ-Ni_3Nb and/or η-Ni_3Ti phases are observed in this alloy. Previous studies on Alloy 718Plus, with chemical composition close to VDM Alloy 780, revealed that phase discrimination between δ and η particles is not straightforward and requires the use of high-resolution characterization techniques such as HRTEM. This work aims at evaluating the use of EBSD technique with regards to phase identification of these plate-shaped precipitates. Classical indexing of diffraction patterns based on Kikuchi band detection in Hough space fails to differentiate between the two phases. However approaches based on the comparison of experimental and simulated patterns, at least partly, could overcome this issue. The advanced dictionary-based approach that involves the simulation of dynamic electron scattering events identified η phase as the main component of these grain boundary precipitates, consistent with the recently published HRTEM investigation on VDM Alloy 780. Refinement of the classical indexing method under kinematic assumptions implemented in the "Refined Accuracy" mode on the Oxford AZtec software package also led to appreciable improvement.

* Corresponding author.

Email addresses: juhi.sharma@mines-paristech.fr (J. Sharma*), alexis.nicolay@mines-paristech.fr (A. Nicolay), mdg@andrew.cmu.edu (M. De Graef), nathalie.bozzolo@mines-paristech.fr (N. Bozzolo)

1. Introduction

Electron backscattered diffraction (EBSD) is a widely used technique for microstructure and micro-texture characterization. Classical EBSD pattern indexing is based on the angles measured between the Kikuchi bands (that is a gnomonic projection of the angles between the diffracting planes onto the EBSD detector screen) after detecting the band positions in the Hough transform of the pattern. Conventional EBSD can be used efficiently for phase discrimination provided the considered phases have significant differences in their crystal structures and consequently differences in the detected interplanar angles.

The design of polycrystalline nickel-based superalloys is usually adjusted to promote the precipitation of (i) hardening phases and (ii) particles to pin grain boundaries and control grain sizes. Depending on the various alloying elements and the associated chemical composition, different phases can be found in superalloys. There are several examples in these materials where EBSD fails to distinguish between two phases. The γ-γ′ alloy system is one such example which presents a well-known challenge of discrimination between the disordered FCC matrix phase and the ordered $L1_2$ precipitated phase. The lattice parameters of γ and γ′ are often quite close, differing by less than 0.5% [1]. Due to structural similarities, the two phases exhibit very similar diffraction patterns. The weak additional diffracted intensities resulting from the ordered γ′ structure are not sufficient to be detected and used to discriminate between the two phases by EBSD. This problem was overcome in a γ-γ′ nickel-based superalloy by coupling EBSD with Energy dispersive X-ray spectroscopy (EDS) which also allows taking into account the chemical composition of the phases [2]. Only primary γ′ precipitates were large enough to be separated from the matrix based on the EDS signal, EDS spatial resolution being in the range of 1 μm. Another method that could successfully solve this phase discrimination issue in a γ-γ′ nickel-based superalloy [3] was based on the chemical contrast of Secondary ion (SI) images correlated with the crystallographic orientations obtained by the i-CHORD technique [4]. The spatial resolution of SI images allowed for identification of γ′ particles as small as 150 nm.

This article deals with another problem of phase discrimination, between δ and η phases, in nickel-based superalloys where none of the aforementioned approaches work. The crystallographic description and the lattice parameters of the generic compounds of both phases are given in Table 1 [5]. Theoretically, δ phase exists as Ni_3Nb with an orthorhombic structure whereas η-Ni_3Ti has a hexagonal structure as shown in Fig. 1. Owing to their different crystal structures and chemical compositions, δ and η phases seem *a priori* to be easily differentiable; which is actually not true as detailed below.

Table 1
Crystallographic information of δ and η phases [5].

Phase	**δ**	**η**
Generic compound	Ni_3Nb	Ni_3Ti
Unit cell	Orthorhombic – D0a	Hexagonal – $D0_{24}$
Space Group	Pmmn	$P6_3/mmc$
No.	59	194
Lattice parameters, nm	$a = 0.514$, $b = 0.423$, $c = 0.453$	$a = 0.5096$, $c = 0.8304$

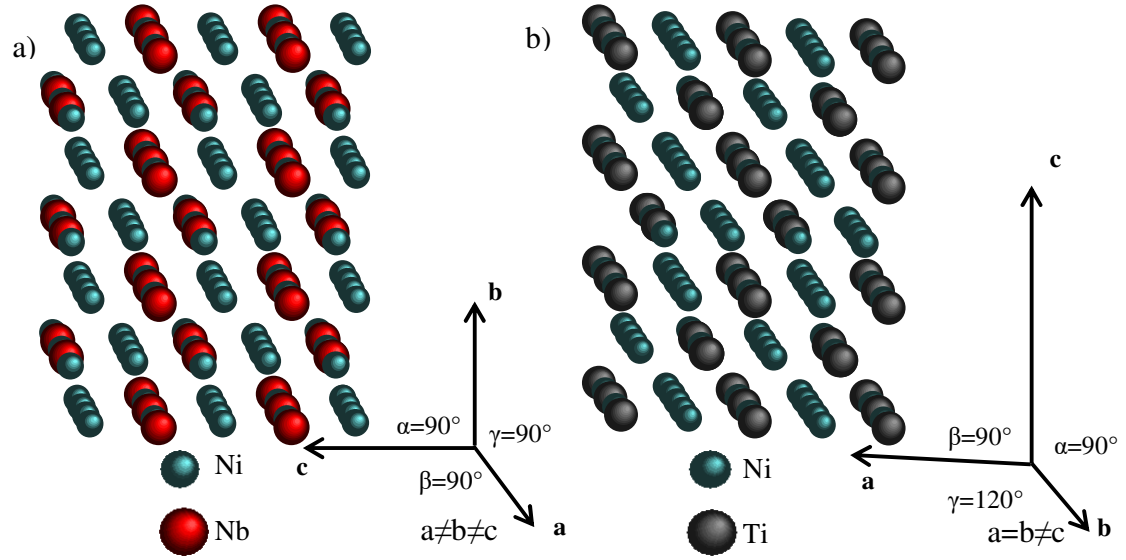

Fig. 1. Crystal structures of a) δ-Ni_3Nb and b) η-Ni_3Ti where $[010]_\delta \parallel [0001]_\eta$.

Both δ and η phases precipitate discontinuously at the grain boundaries and result in serrated boundaries [6]. The two phases usually display similar needle/plate-type morphology. These phases are characterized by a γ′-precipitate depleted zone around them as a result of local variation in the alloying element contents as observed in Alloy 718Plus [6, 7] and in VDM Alloy 780 (Fig. 2). Topologically, both phases resemble each other.

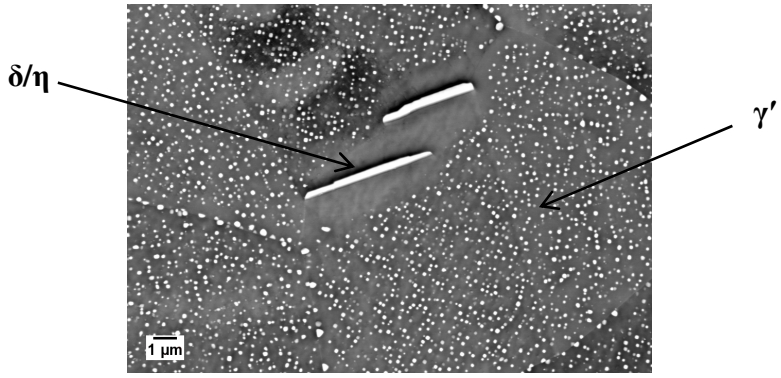

Fig. 2. Backscattered electron image (BSE) showing γ′-depleted zone around needle/plate-shaped particle in VDM Alloy 780 heat treated at 960°C for 10 hours.

Moreover, they can actually exist with similar compositions by substituting the elements present in their generic structure compounds which make the use of chemical information insufficient to recognize their precise nature. TEM/EDS (Transmission electron microscope coupled with Energy dispersive X-ray spectroscopy) indeed revealed the presence of a plate-like phase $Ni_3Al_{0.5}Nb_{0.5}$ with a hexagonal structure similar to that of η-Ni_3Ti but rich in Nb and Al and not Ti [8]. In another study, the same technique showed affinity of Nb, Al and Ti towards η phase and η-Ni_6AlNb was seen to form with its majority of Ti sites replaced by Al and Nb while conserving the hexagonal structure [6]. TEM/EDS analysis on the same alloy discussed presence of δ phase which deviated from the generic Ni_3Nb stoichiometry and contained Nb, Al and Ti [7]. Because of the common forming elements (Nb, Al and Ti) in the two phases, chemical composition cannot really help to distinguish between δ and η phases. In addition, it is worth mentioning that SEM/EDS (EDS in a Scanning electron microscope) should anyway be avoided in such phase

identification issues as the thickness of these lamellar particles is usually below the spatial resolution of SEM/EDS.

Therefore, crystallographic information has to be taken into consideration in this context. Precipitation of δ-Ni_3Nb phase in Inconel 718 is well-known and has been demonstrated in the literature using TEM with an orientation relationship to the γ matrix: $\{111\}_\gamma // (010)_\delta$ and $\langle 1\bar{1}0\rangle_\gamma // [100]_\delta$ [9-12]. HRTEM (High resolution transmission electron microscopy) study on Inconel 718 has also revealed presence of a local stacking fault of type (ABA<u>C</u>AB…) within δ (ABCABC…) structure [13]. This kind of stacking fault can also be seen as a local η layer but concerning only three atomic planes. No example of thicker η layer defects observed in the δ phase of Inconel 718 could be found in the literature.

However, in case of more recently developed alloys such as Alloy 718Plus and VDM Alloy 780, phase identification of the grain boundary precipitates has posed challenges. X-ray diffraction (XRD) diagrams showed that the peaks corresponding to the grain boundary precipitates could be assigned to either δ phase, η phase or $Ni_3Al_{0.5}Nb_{0.5}$ phase in Alloy 718Plus [8] and in VDM Alloy 780 [14]. TEM selected-area electron diffraction patterns (SADPs) of the lamellar precipitates in Alloy 718Plus matched the η-Ni_3Ti $D0_{24}$ hexagonal structure [6]. This phase was referred as Ni_6AlNb and was found to have a crystallographic orientation relationship with the γ matrix: $\{11\bar{1}\}_\gamma // (0001)_\eta$ and $\langle 1\bar{1}0\rangle_\gamma // \langle 2\bar{1}\bar{1}0\rangle_\eta$ with lattice parameters similar to those of η-Ni_3Ti. Another study on Alloy 718Plus described the presence of fine δ atomic layers as faults in the local stacking sequence of the η structure using HAADF-STEM (High angle annular dark field imaging in a Scanning transmission electron microscope) [15]. A more recent study on VDM Alloy 780 using HRTEM also showed that the plate-shaped particles are composed of alternating layers of η and δ phases following the crystallographic orientation relationship: $(0001)_\eta // (010)_\delta$, $\{10\bar{1}0\}_\eta // (001)_\delta$, $\langle 2\bar{1}\bar{1}0\rangle_\eta // [100]_\delta$ [16]. This study analyzed samples from two types of heat treatments to generate different microstructures. The first sample was heat treated at 1000°C followed by another heating of 975°C for 16 hours. The other sample was exposed to multiple step ageing treatments at relatively lower temperatures starting from 900°C for 11 hours, then to 955°C for 1 hour followed by ageing at 800°C and 650°C for 8 hours respectively [16]. Both the samples revealed η phase as the principle phase, almost twice that of δ, although both η and δ phases co-existed in all the analyzed particles. Formation of δ phase at the interface of the plate-shaped particle was also observed in the sample exposed to the multiple step ageing treatments at lower temperatures. Relatively thicker δ phase stripes (20-50 nm) were encountered in this study as compared to that in Alloy 718Plus where δ stripes were narrower [15].

The effect of chemical composition on the formation of δ and η phases has been demonstrated by considering different experimental alloys [17]. It was empirically shown that the tendency of an alloy to form δ and/or η phases can be influenced by the atomic ratio of (Nb+Ta) / (Al+Ti) [17]. According to this study, a ratio of less than 1 favors η phase, a ratio well above 1 ensures δ phase, whereas a ratio close to 1 generates a microstructure with both δ and η phases. For Alloy 718, this ratio is 1.55 and indeed exhibits presence of δ phase [17]. This ratio is 0.86 for Alloy 718Plus [17] and 0.87 for VDM Alloy 780 [14]. Hence both the alloys lie in the η phase domain yet close to δ/η limit. From this compositional tendency, η phase seems more likely to be present in VDM Alloy 780. This is consistent with the HRTEM investigation which showed the main phase in this alloy as η phase [16].

TEM based techniques were thus able to identify the precise nature of these grain boundary precipitates in Alloy 718Plus and VDM Alloy 780 but involved preparation of thin foils and hence are more time intensive, in addition to having the drawback of limited statistics regarding the number of analyzed particles which is inherent to TEM investigations. This article focusses on the issue of phase identification between δ and η phases using EBSD technique, thus with simpler sample preparation and potential for better statistics, in VDM Alloy 780. However, since conventional EBSD indexing could not discriminate between both the phases, advanced indexing methods that rely on the comparison of experimental and

simulated patterns were evaluated and will be shown below to be able to identify the major component of these plate-shaped particles.

2. Material: VDM Alloy 780

The use of nickel-based superalloys in the aerospace industry is extensive owing to their excellent properties at elevated temperatures. The need and demand to increase the maximum operating temperature to reduce emission levels has motivated the development of new superalloys. With this objective, VDM Alloy 780 was developed to achieve improved microstructural stability and service temperature up to 750°C [18, 19]. The chemical composition in Table 2 ensures the microstructure to be predominantly strengthened by γ′ precipitates. Another phase that resembles δ (orthorhombic $D0_a$) and/or η (hexagonal $D0_{24}$) was observed mainly at the grain boundaries (Fig. 3a). The analyzed sample was taken from a VDM Alloy 780 pancake forged from a billet at 1000°C and then heat treated at 980°C for 48 hours. This is comparable to one of the heat treatments applied in the previously reported HRTEM study [16]. This particular heat treatment was chosen in order to obtain a microstructure with considerable amount of such grain boundary precipitates. The three-dimensional shape of these grain boundary precipitates is reconstructed using FIB nano-tomography in Fig. 3b.

Table 2
Nominal chemical composition (wt.%) of VDM Alloy 780, Alloy 718Plus and Alloy 718.

Alloy	Al	Ti	Cr	Fe	Co	W	Nb	Mo	Ni
VDM Alloy 780	2	0.3	18.0	<3	25.0	--	5	3.0	Bal.
Alloy 718Plus	1.45	0.75	18.0	9.5	9.1	1.0	5.4	2.7	Bal.
Alloy 718	0.6	0.9	19.0	18.5	--	--	5.15	3.0	Bal.

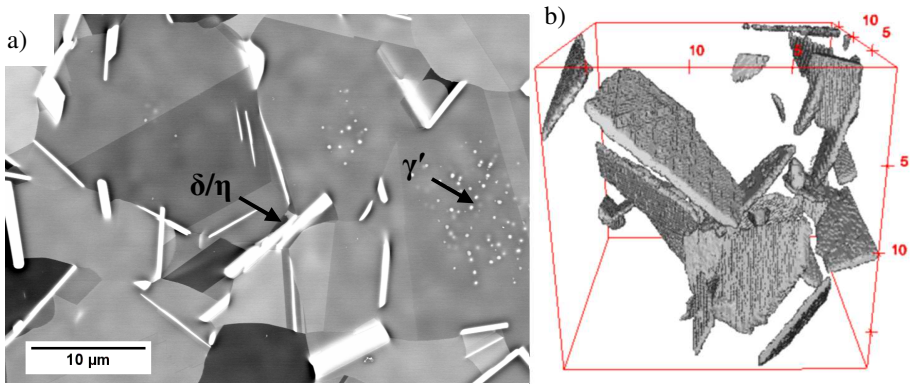

Fig. 3 a) Microstructure of VDM Alloy 780 after a heat treatment at 980°C for 48 hours showing presence of γ′ (spheroid-shaped) and δ/η precipitates (plate-shaped), BSE image of a mirror polished sample and b) Three-dimensional view of the plate-shaped particles obtained using Plasma-FIB nano-tomography (in a Tescan FERA3 microscope) on a volume of 17.5x17.5x17.5 μm^3 with a cubic voxel size of 100 nm.

3. Reason why conventional EBSD fails in δ/η phase discrimination

The experimental electron backscattered pattern (EBSP) of a δ/η particle (arrowed on Fig. 4a) is shown in Fig. 4b. This pattern could be indexed "classically" based on the angles measured between the Kikuchi bands detected in the Hough transform of the pattern, using the crystallographic data of either orthorhombic δ-Ni_3Nb or hexagonal η-Ni_3Ti phase. Two commercial EBSD systems have been tested (C-Nano detector coupled with AZtec software from Oxford and e-Flash detector coupled with Esprit

software from Bruker). Both systems led to the same conclusion: an experimental pattern (Fig. 4b) could be successfully indexed using crystallographic data of δ-Ni_3Nb and of η-Ni_3Ti phases, as shown in Fig. 4c and Fig. 4d respectively.

Both solutions appear similar even though minute differences exist (marked by yellow lines on Fig. 4c) which suggest that the pattern more likely corresponds to η-Ni_3Ti phase. However these differences are too subtle to help in phase discrimination in an automatic Hough transform-based indexing procedure. The mean angular deviation (MAD) which measures the misfit between the detected bands and those of the proposed solutions are very close in both cases. Using the Oxford AZtec software package, the MAD of the example shown in Fig. 4 was calculated as 0.19° considering δ-Ni_3Nb and 0.17° when considering η-Ni_3Ti with 12 identified bands in both cases. This similarity between the diffraction patterns of δ and η phases can actually be understood when looking at the crystal structures plotted in Fig. 1. Crystal lattices are aligned according to the misorientation between δ and η phase in accordance to the pattern indexing shown in Fig. 4 which is also consistent with the previously reported orientation relationship: $(\mathbf{0001})_{\eta}$ // $(\mathbf{010})_{\delta}$, $\{\mathbf{10\bar{1}0}\}_{\eta}$ // $(\mathbf{001})_{\delta}$, $\langle\mathbf{2\bar{1}\bar{1}0}\rangle_{\eta}$// $[\mathbf{100}]_{\delta}$ [16].

Both structures look similar in terms of arrangement of atoms and differ only by slight distortions which make them fall into either orthorhombic or hexagonal crystallographic system. Diffracting planes in both these phases form almost the same angles between them. The difference in those angles in one phase compared to the other is likely to be within the tolerance that must be admitted in the classical EBSD indexing procedure. This explains why conventional EBSD fails in discriminating between δ and η phases.

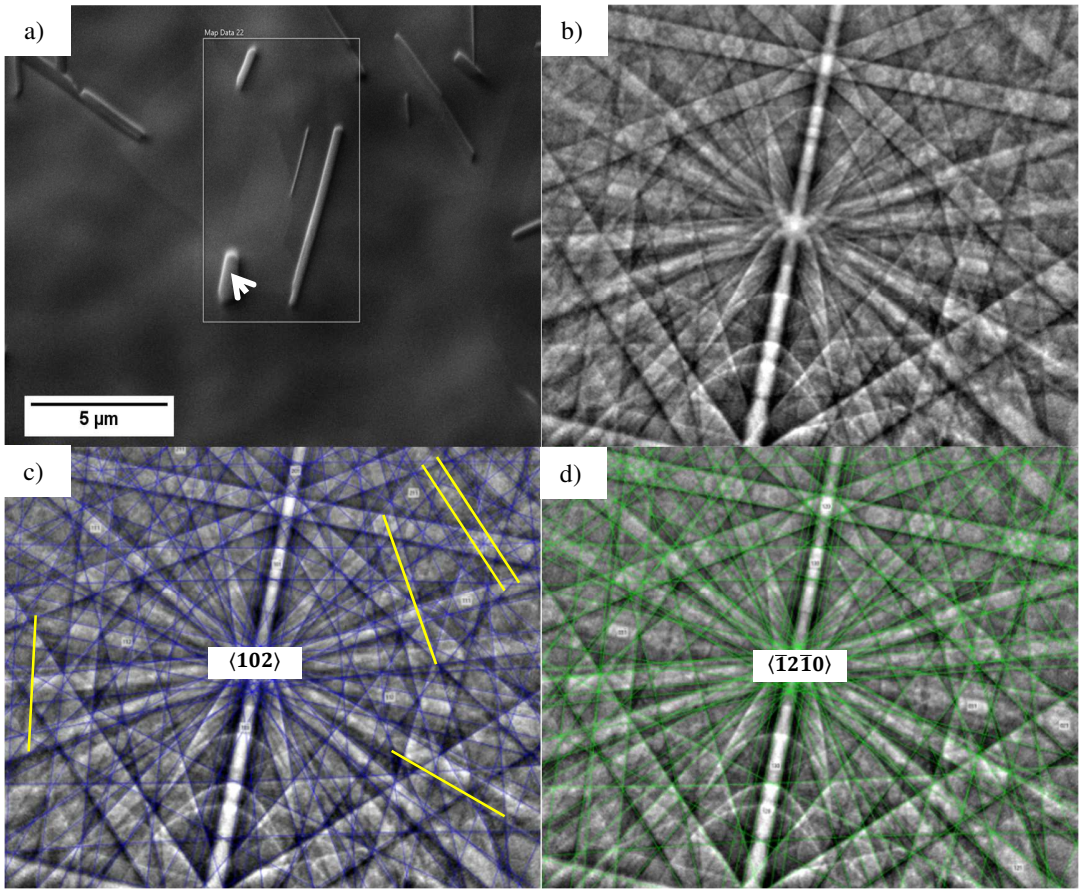

Fig. 4. a) Forward scattered electron (FSE) image showing the δ/η particle (white arrow) under investigation, b) Experimental EBSD pattern of the particle, c) Experimental pattern indexed using

orthorhombic δ-Ni_3Nb data with $\langle \mathbf{102} \rangle_{\boldsymbol{\delta}}$ zone axis at the center of the particle, and d) Experimental pattern indexed using η-Ni_3Ti crystallographic data with $\langle \bar{\mathbf{1}}\mathbf{2}\bar{\mathbf{1}}\mathbf{0} \rangle_{\boldsymbol{\eta}}$ zone axis at the center. Yellow lines on c) highlight missing lines as compared to d).

4. Comparison of conventional and more advanced EBSD indexing methods

A sample of VDM Alloy 780 (annealed at 980°C for 48 hours, same as in Fig. 3) was analyzed by EBSD using a Tescan FERA3 Field emission gun scanning electron microscope (FEG-SEM) equipped with an Oxford EBSD system comprising a C-Nano detector and AZtec software package. The settings used for the analyses are given in Table 3. Two different indexing modes available on the Oxford AZtec software package were used: (i) Optimized indexing mode based on classical Hough transform and (ii) "Refined Accuracy" mode. The same sets of patterns were analyzed using the Dictionary Indexing method implemented in the open source EMsoft software package. All these three approaches are further described below.

Table 3
Parameters used in phase identification using EBSD.

Parameter	Value
Working distance	23.2 mm
Accelerating voltage	15 kV
Sample tilt	70°
EBSD detector gain	1
EBSP size	311×256 pixels
Integration time per frame	8 ms
Step size	0.1 μm

4.1 Conventional Hough transform based indexing

Conventional EBSD uses the Hough transform of the pattern to detect the position of Kikuchi bands and determine the angles between each pair of bands. From the list of measured angles and assuming a given crystal structure, the software determines the possible crystal orientation giving rise to the recorded band configuration. The accurate identification of the phase and orientation of the crystal depends mostly on the precise detection of these band positions. This, in turn, depends on the resolution of the Hough space and on the mask-filter used for band detection in the Hough space in addition to the contrast, sharpness and resolution of the pattern image itself.

4.2 Dictionary Indexing (DI)

Contrary to the classical Hough transform approach that only aims at detecting bands, the DI method uses all the available pixels rather than only linear aspects of the diffraction pattern image [20-22]. DI uses a library of precomputed simulated patterns to index the experimental diffraction patterns with best match from the dictionary. For this purpose, a normalized dot product between the experimental patterns and dictionary elements is used to determine the best match and the orientation of the corresponding dictionary element. A physics-based forward model is used for computation of the dynamic electron-scattering events in the form of a master Kikuchi pattern. The individual diffraction patterns are obtained using bi-linear interpolation of these master patterns [20]. The master patterns of δ and η phases in Fig. 5 confirm the similarity of both phases with regards to diffraction signals. Slight relative intensity modulations and fine differences in the angles between bands exist between these phases which can barely be detected by simple visual inspection.

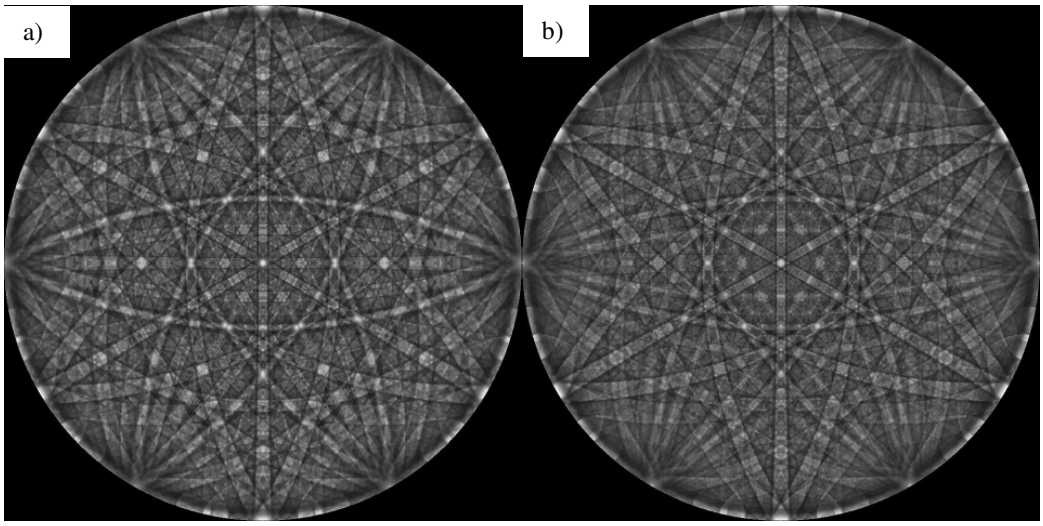

Fig. 5. Master patterns at 20 kV for a) δ-Ni_3Nb with orthorhombic [010] axis in the middle of the pattern and b) η-Ni_3Ti with [0001] axis in the middle of the pattern consistent with the alignment of the crystal structures in Fig. 1 and that arising from pattern indexing in Fig. 4.

4.3 "Refined Accuracy" method offered by the Oxford system

Within the Oxford AZtec software package, the orientation measurement accuracy can be improved by using the so-called "Refined Accuracy" mode that also uses simulated Kikuchi patterns but calculated under kinematical assumptions [23]. In the "Refined Accuracy" mode, an experimental pattern is first indexed using a variant of the classical Hough transform. Band detection in Hough space is performed with a sub-pixel resolution allowing to detect the position of the bands with a precision which is slightly improved compared to the classical Hough transform indexing. This first solution is then used to model, under kinematical assumption, the expected band edge positions taking into consideration their hyperbolic shape. The refined solution is then determined as the best fit between the simulated and the original experimental pattern [24]. This corresponds to the so-called refinement step that enables better determination of the band positions and hence can be used to discriminate between some phases with similar crystal structures [25, 26].

5. Results and Discussion

Conventional EBSD based on classical Hough transform could not differentiate between δ and η phases as seen from Fig. 6b where most of the particles contain pixels corresponding to both δ and η phases with poor spatial correlation. It is worth noting that both δ and η phases can be indexed using the crystallographic information in Table 1 even though their actual chemical composition deviates from the generic compounds. The pole figures in Fig. 6c indicate that points indexed as η and δ phases follow the aforementioned orientation relationship (section 1) with γ-matrix, which is also summarized in Table 4.

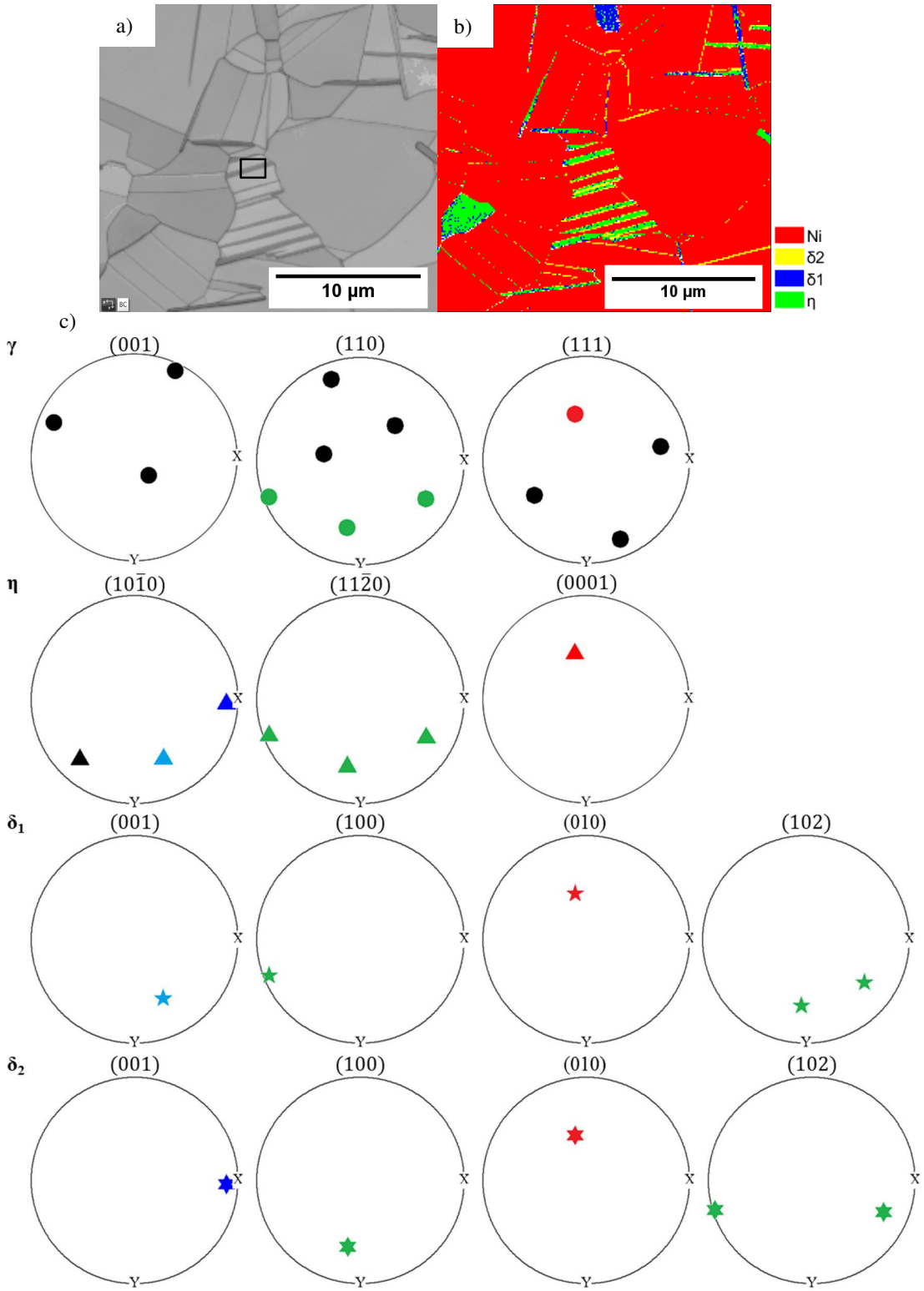

Fig. 6. a) Band contrast image of the area indexed using conventional Hough transform based indexing, b) associated phase map, and c) Pole figures for γ, η and δ phases corresponding to the region (black box) shown in a). The colors aim at highlighting alignment of different poles of corresponding phases.

Table 4
Aligned crystallographic planes and directions of γ, η and δ phases from pole figures in Fig. 6c.

Phase	Planes Aligned		Direction Aligned		Symbol
γ phase	{111}		<110>		circle
η phase	(0001)	$(11\bar{2}0)$	$<11\bar{2}0>$	$<10\bar{1}0>$	triangle
δ phase	(010)	(100)	[100], [102]	[001]	star

A set of diffraction patterns acquired with the Oxford C-Nano detector on a region involving δ/η particles (white box in Fig. 7a) were saved and analyzed using the Dictionary Indexing method. Conventional EBSD generated a phase map given in Fig. 7b with mixed δ/η indexing. The points near the matrix/particle interface seem to have a higher mixed-indexing rate. Fig. 7c shows the phase map obtained using Dictionary Indexing. Firstly, indexing has been performed for one phase at a time. A line profile map (see Fig. 7d) for the same region displays the maximum refined dot product values for δ, η and γ phases. This normalized dot product determines the best match and orientation for the experimental pattern; it is systematically higher for η phase as compared to δ phase. Fig. 7c was generated by considering all the three phases for each pixel and selecting the phase with the highest value of this refined dot product.

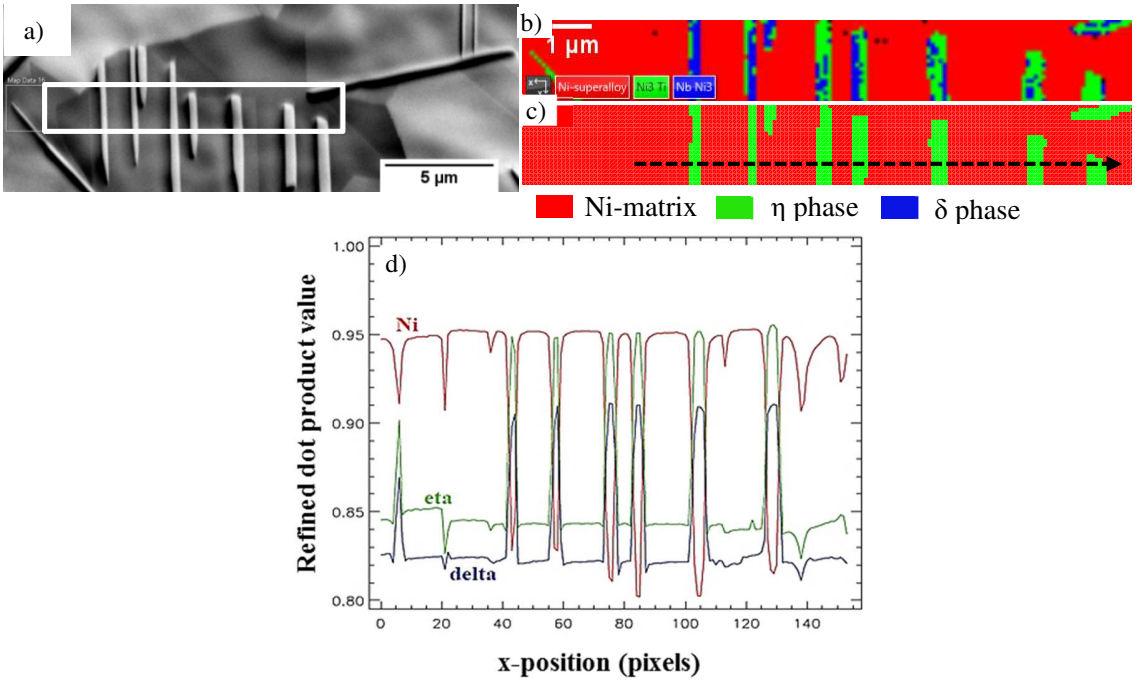

Fig. 7. a) FSE image showing the analyzed area (white box), b) Phase map obtained with conventional Hough transform based indexing, c) Phase map obtained using DI technique, and d) Line profile through the particles (dotted line on c) showing refined dot product values for δ, η and γ phases.

Contrary to the classical indexing technique, Dictionary Indexing showed that all the points in particles of the analyzed area are most likely to be η phase. The result from DI method is consistent with the chemical composition criterion leading to the occurrence of η phase mentioned in section 1 [17] and with the HRTEM investigations which identified η as the major phase in VDM Alloy 780 [16]. However, the presence of thin layers of another phase precisely observed by the HRTEM studies could not be resolved using EBSD, despite the fact that the analyzed area was chosen to get the best possible spatial resolution through the thickness of the plates (i.e. with the long dimension of the particle aligned with the Y direction

of the map). The typical spatial resolution of EBSD in a FEG-SEM is indeed better, in the order of 30 nm along the X direction parallel to the tilt axis and about three times lower, about 100 nm, in the Y direction [27] because of the geometric configuration with the analyzed surface tilted by 70°.

In Alloy 718Plus, the stacking defects of δ phase observed within η structure were only few tens of nanometers in thickness [15]. For VDM Alloy 780, these δ layers had a thickness of 20-50 nm inside η [16], about the expected EBSD spatial resolution along the X direction. There is thus only a slight possibility that the thin δ phase layers could be resolved, which would require them to be lying perpendicular to the scanned surface. Such thin δ layers could actually not be revealed using the DI method in the analyzed region.

The two different EBSD indexing modes available on the Oxford AZtec software package described in section 4 were compared to Dictionary Indexing results on another area as shown in Fig. 8a. DI again revealed the analyzed particles as η phase (see Fig. 8b), except the particle marked as A which was obviously too thin to be resolved under the actual settings. Conventional EBSD settings generated the phase map in Fig. 8c with mixed indexed points of δ and η phases; with higher proportion of δ phase in particle B, higher proportion of η phase in particle C, a core of η surrounded by δ in particle D. Analyzing the same area using "Refined Accuracy" mode (Fig. 8d) significantly changed the results. The lamellar particles (see Fig. 8d) now appear more likely to be η phase although a number of (sparse) points, notably close to the matrix/particle interfaces, are still indexed as δ phase. Noteworthily, few points at grain or twin boundaries of the matrix are also misindexed as either η or δ phase.

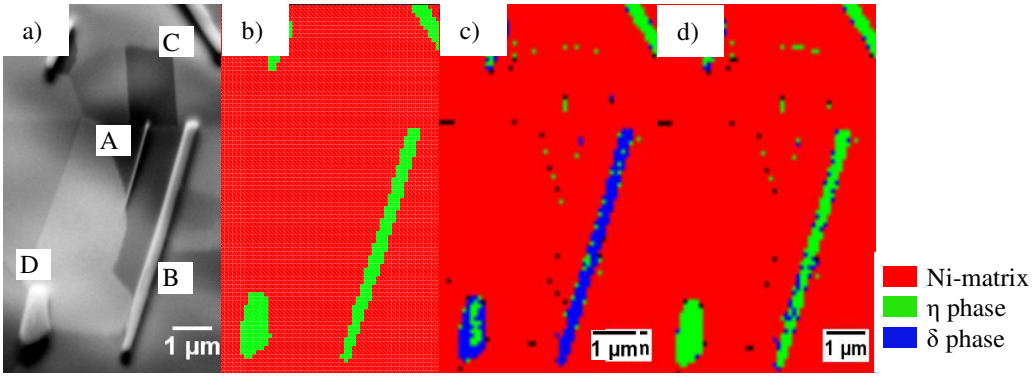

Fig. 8. a) FSE image of the analyzed particles, b) Phase map using DI, c) Phase map using conventional indexing mode, and d) Phase map using "Refined Accuracy" mode.

A possible explanation for points indexed as δ phase at the interface between the particle and the matrix could be the actual presence of a δ interfacial layer, as earlier reported by the HRTEM analyses on VDM Alloy 780 sample submitted to multiple heat treatment steps at lower temperatures (900°C for 11 hours, then to 955°C for 1 hour followed by ageing at 800°C and 650°C for 8 hours respectively) [16], and in an Alloy 7180Plus sample heat treated at 840°C for 72 hours [15]. But this explanation most probably is not suitable in the present case since DI method with the exact same set of diffraction patterns did not return such interfacial δ phase points or internal thin defect layers. It is thus more likely that these points are actually misindexed as a result of poorer diffraction pattern quality as a result of a combination of diffraction intensities coming from both particle and matrix. Pattern overlapping would also explain the misindexed η or δ phase points at the grain and twin boundaries.

In order to check the latter hypothesis, the "Refined Accuracy" mode on the Oxford system was also used to analyze a sample of Inconel 718. Presence of δ phase in Inconel 718 is well-known and has been reported in several studies [9-12]. In the δ phase of this alloy, the presence of stacking faults of η type has been reported however their thickness is far below the spatial resolution of EBSD. Fig. 9b confirms the

presence of δ phase in all the analyzed particles. However, some points at the particle/matrix interface are indexed, actually misindexed, as η.

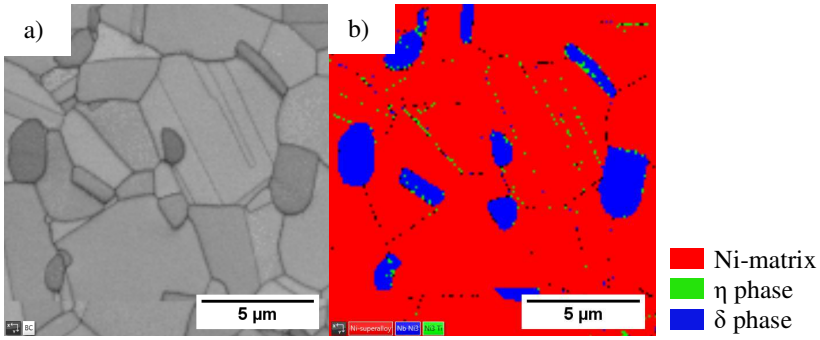

Fig. 9. a) Band contrast image of Inconel 718 and b) Phase map using "Refined Accuracy" mode.

One of the possible solutions to handle overlapping diffraction patterns at the particle/matrix interface or due to the lack of spatial resolution of the thin layers of a phase within another, could be to use the DI method with a combination of overlapping master patterns as done in the case of α and β phases in titanium alloy [28]. The same principle could be applied here since the orientation relationships between the involved δ, η and γ phases are known and well-defined and could thus be used to produce suitable overlapping master patterns. This is a perspective to the work presented here.

6. Conclusion

δ and η phases cannot be easily distinguished in nickel-based superalloys based on their shape or chemical composition alone. Despite their different crystallographic systems (orthorhombic for δ phase and hexagonal for η phase), conventional EBSD fails to discriminate between δ and η phases. This is due to the underlying similarities in terms of atomic arrangements and associated diffraction signals.

HRTEM study on this alloy has revealed that these plate-shaped particles are actually composed of alternating layers of δ phase within η phase, with η almost twice that of δ phase [16]. The present work attempts to solve the issue of phase identification using advanced EBSD indexing methods. In this context, the advanced Dictionary Indexing technique appeared to be able to index all the analyzed particles as η phase in VDM Alloy 780. The "Refined Accuracy" indexing mode available on the Oxford AZtec software was also able to identify the particles as η phase, except for the points close to the grain boundaries.

However, these advanced indexing techniques were able to identify only the major component (η phase) of the grain boundary precipitates in this alloy. The very possible presence of fine layers of δ phase within η phase, reported in the literature using HRTEM, could not be resolved using these techniques. The use of DI method with overlapping master patterns could potentially allow overcoming this drawback. Nevertheless, the possibility of discriminating between η and δ phases in superalloys without requiring TEM based techniques is by itself a step forward, avoiding complex preparation of thin foils, opening the route for better statistics in terms of the number of analyzed particles and being less time-intensive.

Acknowledgements

Authors wish to thank VDM Metals GmbH for funding this work and providing the material for this study. MDG acknowledges funding from a DoD Vannevar-Bush Faculty Fellowship (N00014-16-1-2821), as well as the computational facilities of the Materials Characterization Facility at CMU under grant # MCF-677785.

Data availability: Raw/processed EBSD data can be made available on request.

References

[1] B. El-Dasher, A. Deal, Application of electron backscatter diffraction to phase Identification, in: A. J. Schwartz, M. Kumar, B. L. Adams, and D. P. Field (Eds.), Electron Backscatter Diffr. Mater. Sci, Springer US, Boston, MA (2009) 81–95, https://doi.org/10.1007/978-0-387-88136-2_6.

[2] M. A. Charpagne, P. Vennéguès, T. Billot, J. M. Franchet, N. Bozzolo, Evidence of multimicrometric coherent γ′ precipitates in a hot-forged γ–γ′ nickel-based superalloy, J. Microsc.263 (2016) 106–112, https://doi.org/10.1111/jmi.12380.

[3] S. Vernier, Jean-Michel Franchet, M. Lesne, T. Douillard, J. Silvent, C. Langlois, N. Bozzolo, iCHORD-SI combination as an alternative to EDS-EBSD coupling for the characterization of γ-γ′ nickel-based superalloy microstructures, Mater. Charact. 142 (2018) 492–503, https://doi.org/10.1016/j.matchar.2018.06.015.

[4] C. Langlois, T. Douillard, H. Yuan, N.P. Blanchard, A. Descamps-Mandine, B. Van de Moortèle, C. Rigotti, T. Epicier, Crystal orientation mapping via ion channeling: An alternative to EBSD, Ultramicroscopy 157 (2015) 65–72, https://doi.org/10.1016/j.ultramic.2015.05.023.

[5] P. Villars, Pearson's Handbook: Desk Edition : Crystallographic Data for Intermetallic Phases, ASM International, Vol 2, 1997.

[6] E. J. Pickering, H. Mathur, A. Bhowmik, O.M.D.M. Messé, J.S. Barnard, M.C. Hardy, R. Krakow, K. Loehnert, H.J. Stone, C.M.F. Rae, Grain-boundary precipitation in Allvac 718Plus, Acta Mater. 60 (2012) 2757–2769, https://doi.org/10.1016/j.actamat.2012.01.042.

[7] K. Löhnert, F. Pyczak, Microstructure evolution in the nickel base superalloy Allvac®718Plus™, 7th International Symposium on Superalloy 718 and Derivatives, 2010, https://doi.org/10.1002/9781118495223.ch67.

[8] X. Xie, G. Wang, J. Dong, C. Xu, W.D. Cao, R. Kennedy, Structure stability study on a newly developed nickel-base superalloy-Allvac® 718plus™, Superalloys 718, 625, 706 and Derivatives TMS (2005) 179–191, https://doi.org/10.7449/2005/superalloys_2005_179_191.

[9] M. Sundararaman, P. Mukhopadhyay, S. Banerjee, Precipitation of the δ-Ni_3Nb phase in two nickel base superalloys, Metall. Trans. A 19A (1988) 453–465, https://doi.org/10.1007/BF02649259.

[10] R. Cozar, A. Pineau, Morphology of γ′ and γ″ precipitates and thermal stability of Inconel 718 type alloys, Metall. Mater. Trans. B (1973) 4, 47-59, https://doi.org/10.1007/BF02649604.

[11] I. Kirman, D.H. Warrington, The precipitation of Ni_3Nb phases in a Ni-Fe-Cr-Nb alloy, Metall. Trans. 1 (1970) 2667-75, https://doi.org/10.1007/BF03037800.

[12] M. Dehmas, J. Lacaze, A. Niang, B. Viguier, TEM study of high-temperature precipitation of delta phase in Inconel 718 alloy, Advances in Materials Science and Engineering (2011), https://doi.org/10.1155/2011/940634.

[13] A. Niang, Contribution à l'étude de la précipitation des phases intermétalliques dans l'alliage 718, PhD thesis, Institut National Polytechnique de Toulouse, Toulouse, 2010.

[14] C. Solís, J. Munke, M. Bergner, A. Kriele, M.J. Mühlbauer, D.V. Cheptiakov, B. Gehrmann, J. Rösler, R. Gilles, *In situ* characterization at elevated temperatures of a new Ni-based superalloy VDM-780 Premium, Metall. Mater. Trans. 49A (2018) 4373-4381, https://doi.org/10.1007/s11661-018-4761-6.

[15] O. M. Messé, J. S. Barnard, E. J. Pickering, P. A. Midgley, C. M. F. Rae, On the precipitation of delta phase in Allvac®718Plus, Philos. Mag. 94 (2014) 1132–1152, https://doi.org/10.1080/14786435.2013.878052.

[16] C. Ghica, C. Solís, J. Munke, A.Stark, B. Gehrmann, M. Bergner, J. Rösler, R. Gilles, HRTEM analysis of the high-temperature phases of the newly developed high-temperature Ni-base superalloy VDM 780 Premium, J. Alloys Compd. 814 (2020), https://doi.org/10.1016/j.jallcom.2019.152157.

[17] S. Antonov, M. Detrois, R. C. Helmink, S. Tin, Precipitate phase stability and compositional dependence on alloying additions in γ-γ′-δ-η Ni-base superalloys, J. Alloys Compd. 626 (2015) 76–86, https://doi.org/10.1016/j.jallcom.2014.11.155.

[18] T. Fedorova, J. Rösler, J. Klöwer, B. Gehrmann, Development of a new 718-type Ni-Co superalloy

family for high temperature applications at 750°C, MATEC Web of Conferences 14 (2014), https://doi.org/10.1051/matecconf/20141401003.
[19] J. Rösler, T. Hentrich, B. Gehrmann, On the development concept for a new 718-type superalloy with improved temperature capability, Metals 9 (2019) 1–20, https://doi.org/10.3390/met9101130.
[20] P. G. Callahan, M. De Graef, Dynamical electron backscatter diffraction patterns. Part I: Pattern simulations, Microsc. Microanal. 19 (2013) 1255–1265,https://doi.org/10.1017/S1431927613001840.
[21] S. Singh, M. De Graef, Dictionary Indexing of Electron Channeling Patterns, Microsc. Microanal. 23 (2017) 1–10, https://doi.org/10.1017/S1431927616012769.
[22] Y. H. Chen, S.U. Park, D. Wei, G. Newstadt, M.A. Jackson, J.P. Simmons, M. De Graef, A. O. Hero, A Dictionary Approach to Electron Backscatter Diffraction Indexing Microsc. Microanal. 21 (2015) 739–752, https://doi.org/10.1017/S1431927615000756.
[23] K. Thomsen, N. H. Schmidt, A. Bewick, K. Larsen, J. Goulden, Improving the Accuracy of Orientation Measurements using EBSD, Microsc. Microanal. 19 (2013) 724–725, https://doi.org/10.1017/S1431927613005618.
[24] C. Penman, K. Schmidt, N.H. Thomsen, Method of electron beam diffraction analysis, US Patent. 9,671,354, 2017.
[25] Oxford Instruments NanoAnalysis, Developments in EBSD, AZoM https://www.azom.com/article.aspx?ArticleID=11771 (accessed on 26 December 2020).
[26] A. Nicolaÿ, J.M. Franchet, J. Cormier, H. Mansour, M. De Graef, A. Seret, N. Bozzolo, Discrimination of dynamically and post-dynamically recrystallized grains based on EBSD data: application to Inconel 718, J. Microsc. 273 (2019) 135–147, https://doi.org/10.1111/jmi.12769.
[27] S. Zaefferer, On the formation mechanisms, spatial resolution and intensity of backscatter Kikuchi patterns, Ultramicroscopy 107 (2007) 254-266, https://doi.org/10.1016/j.ultramic.2006.08.007.
[28] W.C. Lenthe, L. Germain, M.R. Chini, N. Gey, M. De Graef, Spherical indexing of overlap EBSD patterns for orientation-related phases- application to titanium, Acta Mater. 188 (2020) 579-590, https://doi.org/10.1016/j.actamat.2020.02.025.